Climate Dynamics (2005) 25: 415–426
DOI 10.1007/s00382-005-0032-5

Oleg A. Saenko · John C. Fyfe · Matthew H. England

On the response of the oceanic wind-driven circulation to atmospheric CO_2 increase

Received: 15 November 2004 / Accepted: 25 April 2005 / Published online: 12 July 2005

Abstract A global, flux-corrected climate model is employed to predict the surface wind stress and associated wind-driven oceanic circulation for climate states corresponding to a doubling and quadrupling of the atmospheric CO_2 concentration in a simple 1% per year CO_2 increase scenario. The model indicates that in response to CO_2 increase, the position of zero wind stress curl in the mid-latitudes of the Southern Hemisphere shifts poleward. In addition, the wind stress intensifies significantly in the mid-latitudes of the Southern Hemisphere. As a result, the rate of water circulation in the subpolar meridional overturning cell in the Southern Ocean increases by about 6 Sv (1 Sv = 10^6 m^3 s^{-1}) for doubled CO_2 and by 12 Sv for quadrupled CO_2, implying an increase of deep water upwelling south of the circumpolar flow and an increase of Ekman pumping north of it. In addition, the changes in the wind stress and wind stress curl translate into changes in the horizontal mass transport, leading to a poleward expansion of the subtropical gyres in both hemispheres, and to strengthening of the Antarctic Circumpolar Current. Finally, the intensified near-surface winds over the Southern Ocean result in a substantial increase of mechanical energy supply to the ocean general circulation.

1 Introduction

Much attention has been given in recent years to understanding the behavior of the ocean thermohaline circulation in global warming scenarios (e.g., Cubasch et al. 2001). Although intimately connected to and in fact inseparable from the thermohaline circulation, less attention has been given to understanding the behavior of the ocean wind-driven circulation in global warming simulations. From the point of view of global climate, however, it is the circulation in the subtropical gyres, driven essentially by wind stress curl, as well as the wind stress-driven Ekman transport off the Equator which jointly diverge most of the heat from the tropical and subtropical oceans (e.g., see Danabasoglu 1998). Furthermore, the convergence of the wind-driven Ekman transport in the mixed layer and the associated vertical velocity (Ekman pumping) set the shape of isopycnals in the upper ocean (from the base of the mixed layer down to more than 1 km in depth in the subtropical gyres), thereby affecting subsurface geostrophic flows. In addition, in the zonally unblocked region of Southern Ocean, the northward Ekman transport, its subsequent convergence and associated downward pumping effectively removes heat from the surface to the deep ocean (Gregory 2000). Finally, the Ekman transport across lines of constant pressure is an important source of available potential energy in the ocean (Fofonoff 1981; Wunsch 1998).

This study addresses the changes in the wind stress and wind-driven ocean circulation in response to increasing concentration of atmospheric CO_2. Various studies indicate that the changes in sea-level pressure observed over the last few decades might have been caused by human activity (e.g., Gillett et al. 2003; Fyfe 2003; Marshall 2003; Boer et al. 2000). Furthermore, climate projections indicate that anthropogenic changes in the atmospheric circulation may continue into the future, with the potential to significantly affect the ocean circulation. In particular, Fyfe and Saenko (2005, hereafter referred to as FS05) show that in a global climate model forced by changing greenhouse gas (GHG) concentrations, the mean position and strength of the Antarctic Circumpolar Current (ACC) change in response to a changing pattern of surface wind stress.

O. A. Saenko (✉) · J. C. Fyfe
Canadian Centre for Climate Modelling and Analysis,
Meteorological Service of Canada, Victoria, BC, Canada
E-mail: oleg.saenko@ec.gc.ca

M. H. England
Centre for Environmental Modelling and Prediction,
University of New South Wales,
Sydney, NSW, Australia

Following on from FS05, but taking a more global perspective, we consider in this paper the changes in the global oceanic wind-driven circulation in response to increasing concentration of CO_2 in the atmosphere. In particular, we document the warming-induced changes in the wind stress curl, and the associated changes in the horizontal mass transport and Ekman pumping in the ocean. Also considered is the warming-induced changes to the work done by the winds on the oceanic general circulation. Our investigation is based on a coupled model simulation following a simple 1% per year CO_2 increase scenario. The climate states corresponding to the times of doubling and quadrupling of atmospheric CO_2 concentration are compared with the climate state at the reference CO_2 concentration.

This paper is structured as follows. In the next section, we briefly describe the coupled model and the design of experiments, as well as compare the model wind stress to observations. In the third section, we define several quantities which characterize the wind-driven oceanic flow. The fourth section presents the projected changes in these quantities in response to CO_2 increase. The main conclusions are given in the final section.

2 The model simulations and comparison with observations

The model we employ is an updated version of the global climate model developed at the Canadian Centre for Climate Modelling and Analysis (CCCma) (Flato et al. 2000). The major components of the model include a general circulation model of the atmosphere (McFarlane et al. 1992, 2004), and a general circulation model of the ocean (based on GFDL MOM 1, Pacanowski et al. 1993), a dynamic-thermodynamic sea-ice model (Flato and Hibler 1992; McFarlane et al. 1992) and a land surface model (McFarlane et al. 1992, 2004). The atmospheric component has T47 resolution with 31 vertical levels. Wind stress is computed using a wind speed dependent drag coefficient corrected for atmospheric stability (Abdella and McFarlane 1997). The oceanic component has double the horizontal resolution of the atmosphere, with grid points spaced at about 1.86 in longitude and latitude. There are 29 vertical levels in the ocean model. Vertical diffusivity in the ocean is set to a constant value of 0.3×10^{-4} m^2 s^{-1}. The mixing of tracers along isopycnals and the eddy-induced transport of tracers are represented according to Gent and McWilliams (1990), with thickness and isopycnal diffusion coefficients set to 10^3 m^2 s^{-1}. Horizontal viscosity and vertical viscosity are set to 1.4×10^5 m^2 s^{-1} and 2×10^{-3} m^2 s^{-1}, respectively. In the version employed here, the model is flux-adjusted using only time-mean fields of heat and freshwater flux corrections. Both fields are relatively small compared to the corresponding physical fluxes in most oceanic regions, although in some locations, particularly near land, the heat flux correction may reach as much as several tens of watts per meter squared.

The model was first integrated for several centuries with fixed concentrations of atmospheric CO_2, roughly corresponding to year 1985. Next, the model integration was continued with CO_2 increasing at 1% per year. Our analysis concentrates on two 10-year mean climate states. One of these states is centered on the time when CO_2 reaches two times its initial concentration (year 70; referred to as $2\times CO_2$ state or climate), whereas the other state is centered on the time when CO_2 reaches four times its initial concentration (year 140; referred to as $4\times CO_2$ state or climate). In addition, the initial integration with the fixed concentration of CO_2 was continued for 100 years. The climate averaged over the last 10 years of this model integration will be referred to as the Control climate against which the $2\times CO_2$ and $4\times CO_2$ climate states will be compared. When decadal averages from other time periods in the Control solution are used, the present results do not change.

We note that our consideration of the $4\times CO_2$ climate state is also motivated by the IPCC (2001) report, in which some of the future scenarios predict that the level of atmospheric CO_2 may reach 800 ppm by year 2100 (for example, the A2 scenario). Also, our consideration of the transient climate states, rather than steady states typical of $2(4)\times CO_2$ climates, is motivated by the fact that our immediate practical interest lies in what the climate will be in the twenty-first century, during which time it will not likely reach a steady state.

Making a comprehensive comparison of climate model results against observations is not a trivial task. However, for the present study, with a focus on the wind-driven ocean circulation, an assessment of the model performance in terms of wind-stress fields is vital. In the context of the large-scale ocean circulation and climate, two of the most fundamental wind-stress quantities are the zonal wind stress and wind stress curl. Here we briefly assess the ability of the model to reproduce these quantities. Among a variety of observationally-based climatological wind stress products, we select for our comparison the Hellerman and Rosenstein (1983; hereafter HR) and the Trenberth et al. (1989) wind stress data. The latter product is based on the European Centre for Medium-Range Weather Forecasts dataset (hereafter ECMWF).

Figure 1a compares the zonally-averaged components of the zonal wind stress in the model and observations. The largest differences are in the extratropics, although there is also notable disagreement between the climatologies at the extratropical latitudes. In particular, the model simulates stronger (weaker) eastward stress in the Southern Ocean compared to the HR (ECMWF) observational estimates. Alternatively, instead of comparing wind stresses, one can compare Ekman transports. Scaling by the Coriolis parameter (which converts the zonal wind stress into the meridional Ekman transport—see next section) reduces the differences in the mid-latitudes to a mag-

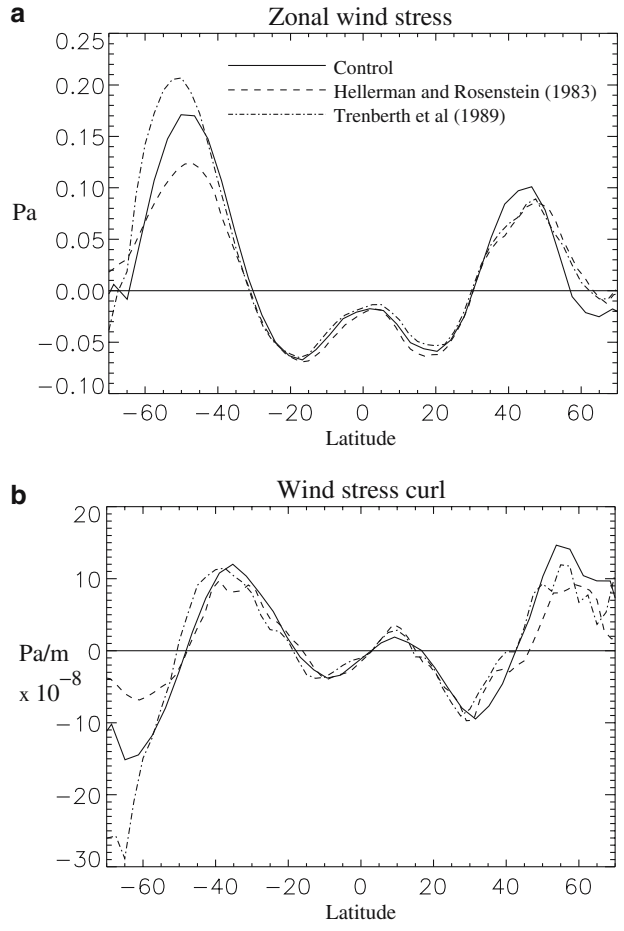

Fig. 1 Zonally-averaged **a** zonal wind stress and **b** wind stress curl in the Control climate, in the Hellerman and Rosenstein (1983) climatology, and in the Trenberth et al. (1989) climatology

nitude comparable to the discrepancies in the tropics (not shown). The model meridional wind stress (and the associated zonal Ekman transport) is in a reasonably good agreement with both observational products (not shown), except in the Northern Hemisphere mid-latitudes where the HR meridional wind-stress is rather weak compared to both the model and ECMWF.

Figure 1b compares the zonally-averaged wind stress curl in the model and observations. In the subtropics and tropics, the input of vorticity to the ocean due to the wind stress curl is well captured by the model. Towards higher latitudes, however, the difference between the model and observations (as well as between the two observational estimates) increases, particularly in the Southern Hemisphere. The HR wind stress likely underestimates the real values over the Southern Ocean due to its bias towards weaker summer values in that region. Overall, the climate model captures the global wind stress and wind stress curl to an accuracy level within the limit of present observational uncertainty.

3 Characteristics of the wind-driven oceanic circulation

In this section we define several quantities that characterize the ocean's wind-driven circulation. Firstly, the Ekman transport vector $\mathbf{U_e} = (U_e^{\lambda}, U_e^{\phi})$ is given by

$$\mathbf{U_e} = \frac{\boldsymbol{\tau}}{\rho_o f} \times \mathbf{k}, \tag{1}$$

where $\boldsymbol{\tau} = (\tau^{\lambda}, \tau^{\phi})$ is the wind stress vector, $\mathbf{k}$ is the unit vector in the vertical, f is the Coriolis parameter, and ρ_o is the reference density of sea water. The superscripts λ, ϕ denote east–west and north–south components, respectively.

The Ekman pumping velocity w_e is given by the divergence of the Ekman transport, i.e.

$$w_e = \nabla \cdot \mathbf{U_e} = \frac{1}{\rho_o f} \mathbf{k} \cdot \left(\nabla \times \boldsymbol{\tau} + \frac{\beta \tau^{\lambda}}{f} \right), \tag{2}$$

where β is the planetary vorticity gradient. Away from the Equator $\nabla \times \boldsymbol{\tau} \gg \beta \tau^{\lambda} / f$, so that the pumping velocity is essentially given by the curl of the wind stress scaled by the planetary vorticity. The Ekman pumping velocity w_e sets the vertical structure of temperature and salinity below the upper mixed layer and down to the base of the pycnocline. In addition, this velocity determines the exchange of mass, heat, salt and other water properties between the surface mixed layer and the subsurface oceanic interior.

In addition to the Ekman pumping, the basin-scale wind stress curl is also responsible for what is known as the oceanic gyre circulation, which is one of the key components of the ocean general circulation and climate. The so-called Sverdrup balance implies a horizontal mass transport streamfunction given by:

$$\Psi(\lambda) = -\int_{\lambda}^{\lambda_E} \frac{\mathbf{k} \cdot \nabla \times \boldsymbol{\tau}}{\rho_o \beta} a \cos\phi \, \mathrm{d}\lambda + \Psi(\lambda_E), \tag{3}$$

where a is the radius of the earth. In Eq. 3, λ_E represents the eastern boundaries of the ocean basins where the value of the mass transport streamfunction, $\Psi(\lambda_E)$, is specified from the corresponding full mass transport. We will illustrate shortly that the Sverdrup transport given by Eq. 3 closely approximates the total horizontal mass transport in our model outside of the zonally unbounded regions of the Southern Ocean and away from the western boundary regions.

The final quantity of interest in our analysis is the Ekman transport across lines of constant pressure. This is given by $\mathbf{U_e} \cdot \nabla p_H$, with ∇p_H being the horizontal surface pressure gradient associated with large-scale ocean circulation. This ageostrophic transport is an important source of available potential energy in the ocean and can be interpreted as a rate of wind work W on the ocean surface geostrophic currents $\mathbf{U_g}$ (Fofonoff 1981), namely

$$W = \mathbf{U_e} \cdot \nabla p_H = \mathbf{U_g} \cdot \boldsymbol{\tau}, \quad (4)$$

where $\mathbf{U_g} = (1/\rho_o f)(\mathbf{k} \times \nabla p_H)$.

4 The oceanic wind-driven circulation under global warming

4.1 Wind stress, the subpolar overturning, and wind stress curl

The zonal wind stress is predicted to change significantly, particularly by the time of CO_2 quadrupling (Fig. 2a). The stress increases poleward of about 45°S and 45°N, whereas it exhibits a weaker decrease equatorward of these latitudes towards the subtropics. Little change is predicted in the zonal mean wind stress at the tropical latitudes (15°S–15°N). We note that the globally-integrated input of angular momentum into the ocean (i.e., $\oint \tau^{\lambda} a \cos\phi \mathrm{d}S$, where S is the area of the ocean surface) is approximately constant despite these large changes in the zonal wind stress. The largest response in the zonal stress is predicted in the Southern Ocean, where the maximum zonal-mean stress increases from 0.17 Pa in the Control to 0.19 Pa at 2×CO_2 and 0.21 Pa at 4×CO_2. In addition, the mean position of the maximum westerly winds shifts poleward by 1–2° in the 2×CO_2 climate and by more than 3° in the 4×CO_2 climate. Although this is not clearly seen in plots of zonal wind stress on the model grid, by fitting the model stress values optimally to a Gaussian shape (not shown) it can be shown that westerly winds in the Southern Ocean do shift poleward as concentration of atmospheric CO_2 increases. This can also be concluded from the shift in the position of zero wind stress curl around 50°S (Fig. 8).

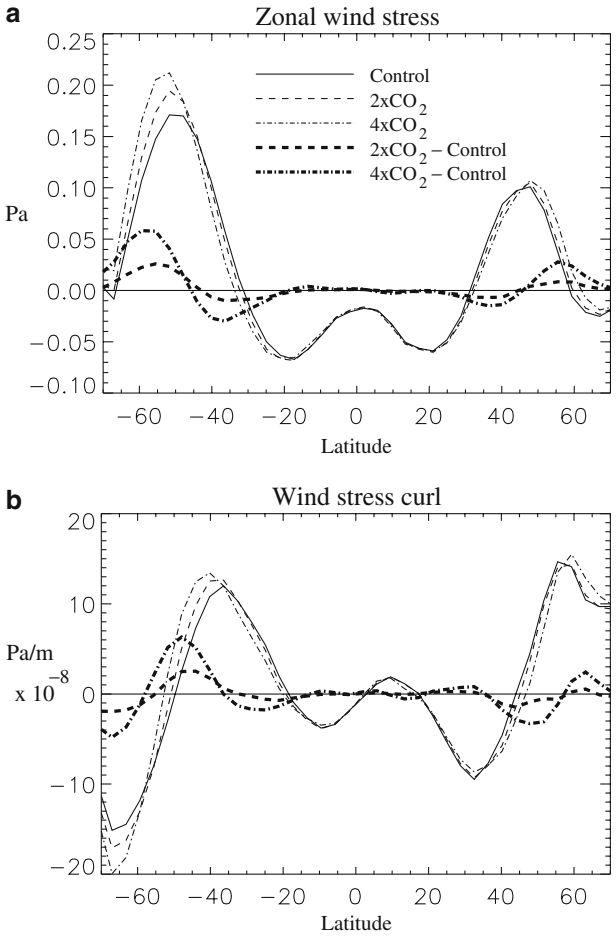

Fig. 2 Zonally-averaged **a** zonal wind stress and **b** wind stress curl in the Control climate, 2×CO_2 climate and 4×CO_2 climate. *Heavy lines* in both panels show the changes (2×CO_2 minus Control; 4×CO_2 minus Control) in the corresponding parameters

We next consider the effect of the intensified zonal wind stress in the Southern Ocean on the subpolar meridional overturning circulation cell, between about 60–40°S. Rather than evaluating this circulation in latitude-depth coordinates, we present it in latitude-density coordinates (Fig. 3). An advantage of using such an approach is described in Döös and Webb (1994) in detail. (Clearly, this cell has both the diabatic and adiabatic components. It is described sometimes as a Deacon Cell (e.g., Speer et al. 2000a, b), whereas in other cases it is only an adiabatic part of this flow which is defined as the Deacon Cell (Döös and Webb 1994). To avoid possible confusion, the term "Deacon Cell" will not be used further.) In the model, the subpolar cell is composed of two circulation cells of opposite sign (Fig. 4). One of them represents the large-scale (Eulerian) circulation, with equatorward flow near the surface within lower density classes and poleward return flow at depth within larger density classes (Fig. 4, left panels). It is called sometimes the "Eulerian circulation cell", a term also employed here. The other cell, which tends to weaken the Eulerian circulation cell, is due to an eddy-induced flow (Fig. 4, right panels). The sum of the two therefore constitutes the subpolar meridional overturning circulation cell as viewed in latitude-density coordinates. In some models of the ocean circulation, this cell essentially disappears (Döös and Webb 1994), whereas in other models it does not (e.g., Speer et al. 2000a; Gregory 2000), as is the case in our model. We note that a complete disappearance of the subpolar cell would imply zero net buoyancy gain (and hence zero net water mass transformation) at the latitudes of the circumpolar flow in the Southern Ocean, which does not seem to be the case according to the available observational estimates (Speer et al. 2000a, b).

As concentration of atmospheric CO_2 increases, the intensified zonal wind stress in the Southern Ocean results in an overall intensification of the subpolar cell (Fig. 3). It can be seen from Figs. 3 and 4 that the intensification of the subpolar cell (by 6 Sv in the 2×CO_2 state and by 12 Sv in the 4×CO_2 state) in the climate change experiments is mostly due to the intensification of the Eulerian circulation cell (Fig. 4, left panels), the strength of which is controlled by the zonal surface winds. The intensified zonal wind stress increases the

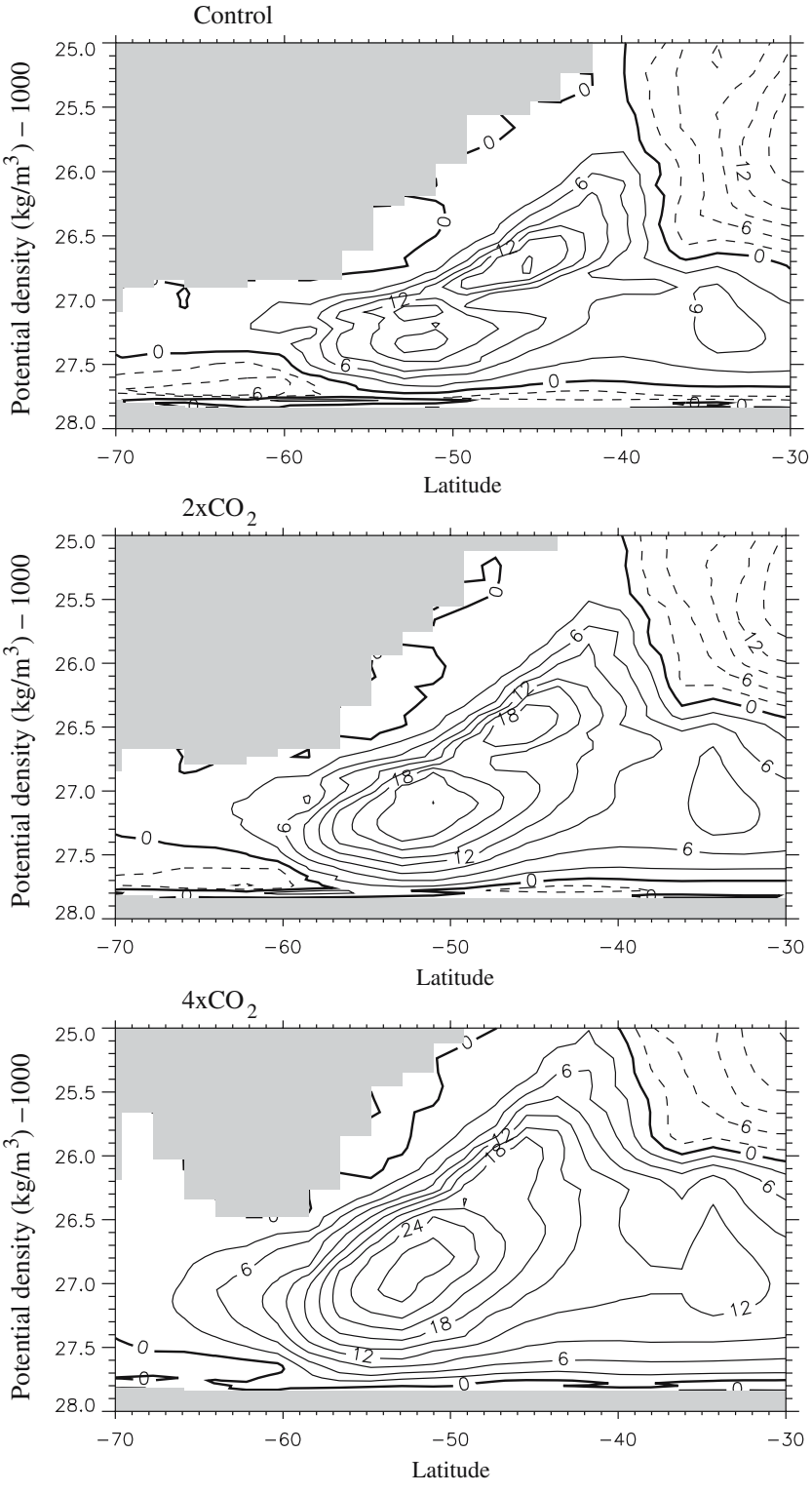

Fig. 3 Total (Eulerian plus eddy-induced) meridional overturning circulation in the Southern Ocean as a function of potential density (*top*) in the Control climate, (*middle*) in the $2\times CO_2$ climate and (*bottom*) in the $4\times CO_2$ climate. Contour interval is 3 Sv; negative values are *dashed*. Clockwise circulation is positive (*solid*)

rate of diabatic flow of relatively light water between 60–40°S, associated with the stronger northward Ekman transport. This is compensated by stronger southward flow of relatively dense water ($\sigma_\theta > 27.4$). In contrast, the intensity of the eddy-induced circulation is not predicted to change significantly over the simulated period (Fig. 4, right panels), as compared to the changes in the Eulerian cell. However, closer consideration indicates that the rate of overturning circulation of the eddy-induced cell does increase non-negligibly, from 15.0 Sv in the Control state to 16.8 Sv in the $4\times CO_2$ state (i.e., by more than 10%), reflecting the associated changes in the

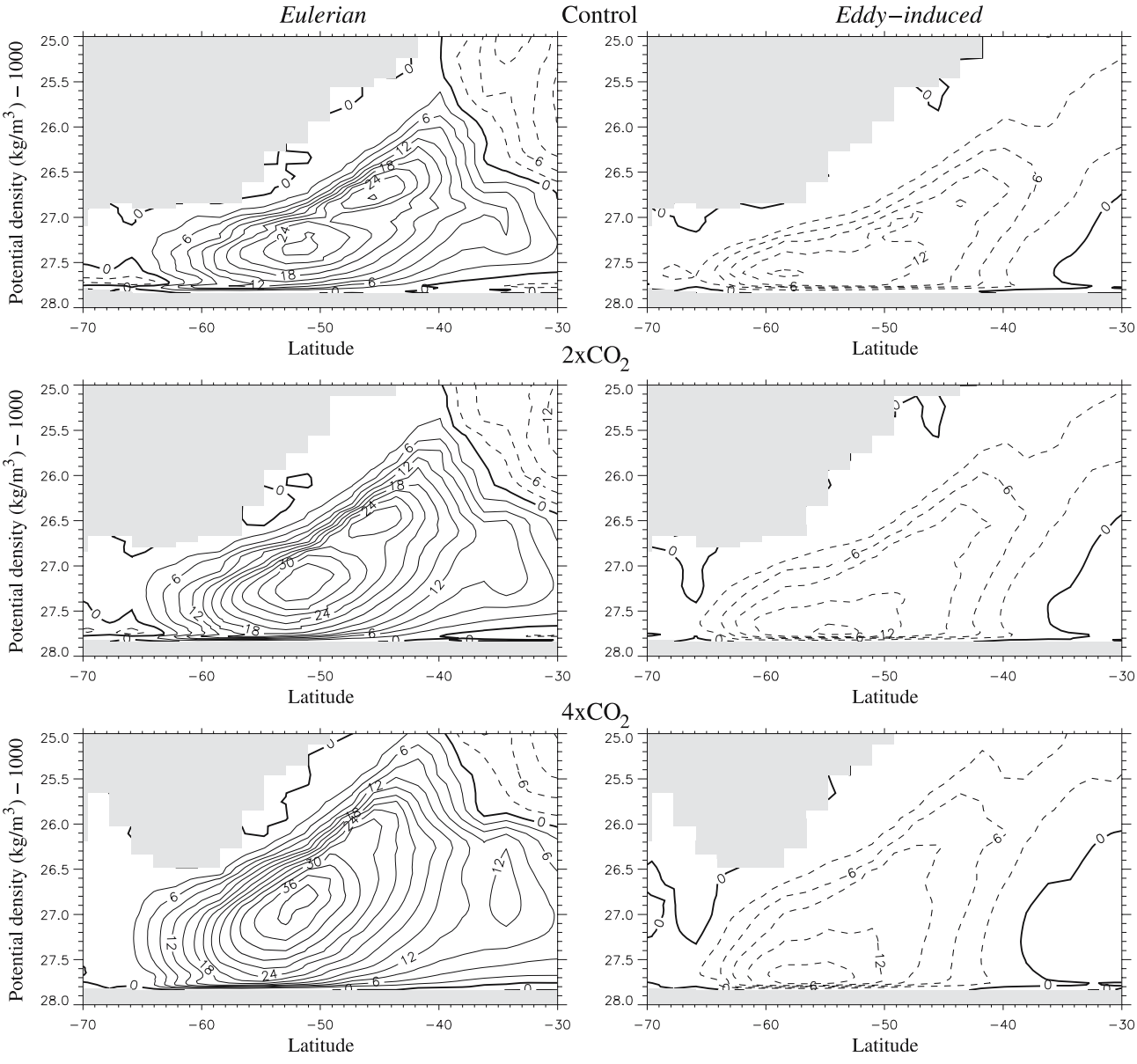

Fig. 4 (*Left*) the Eulerian and (*right*) the eddy-induced meridional overturning circulations in the Southern Ocean as functions of potential density (*top*) in the Control climate, (*middle*) in the 2×CO_2 climate and (*bottom*) in the 4×CO_2 climate. Contour interval is 3 Sv; negative values are *dashed*. Clockwise circulation is positive (*solid*)

oceanic density structure (baroclinicity). The latter, as we shall show, leads to notable changes in the baroclinic potential energy in the Southern Ocean, and hence to associated changes in the ACC transport.

Figure 2b shows the zonally-averaged wind stress curl and its predicted changes. The poleward shift of the position of strong mid-latitude westerlies in both hemispheres results in a poleward shift of the positions of zero wind stress curl at these latitudes. This, according to the Sverdrup balance Eq. 3, is indicative of a poleward expansion (or shift) of the subtropical gyres. The subpolar gyres, by contrast, tend to contract poleward. In turn, the opposite in sign (and smaller magnitude) changes in wind stress curl in the subtropics indicate a reduction of the subtropical gyre transports. We will return to these points in the next section.

4.2 Ekman pumping and horizontal mass transport

The effect of the Ekman transport convergence/divergence in terms of the large-scale oceanic downwelling/upwelling can be seen in Fig. 5a, showing Ekman pumping in the Control simulation. The convergence of the Ekman transport in the subtropics forces downward Ekman pumping, whereas the divergence of this transport in the subpolar regions forces upward Ekman pumping. With the increase of atmospheric CO_2, the

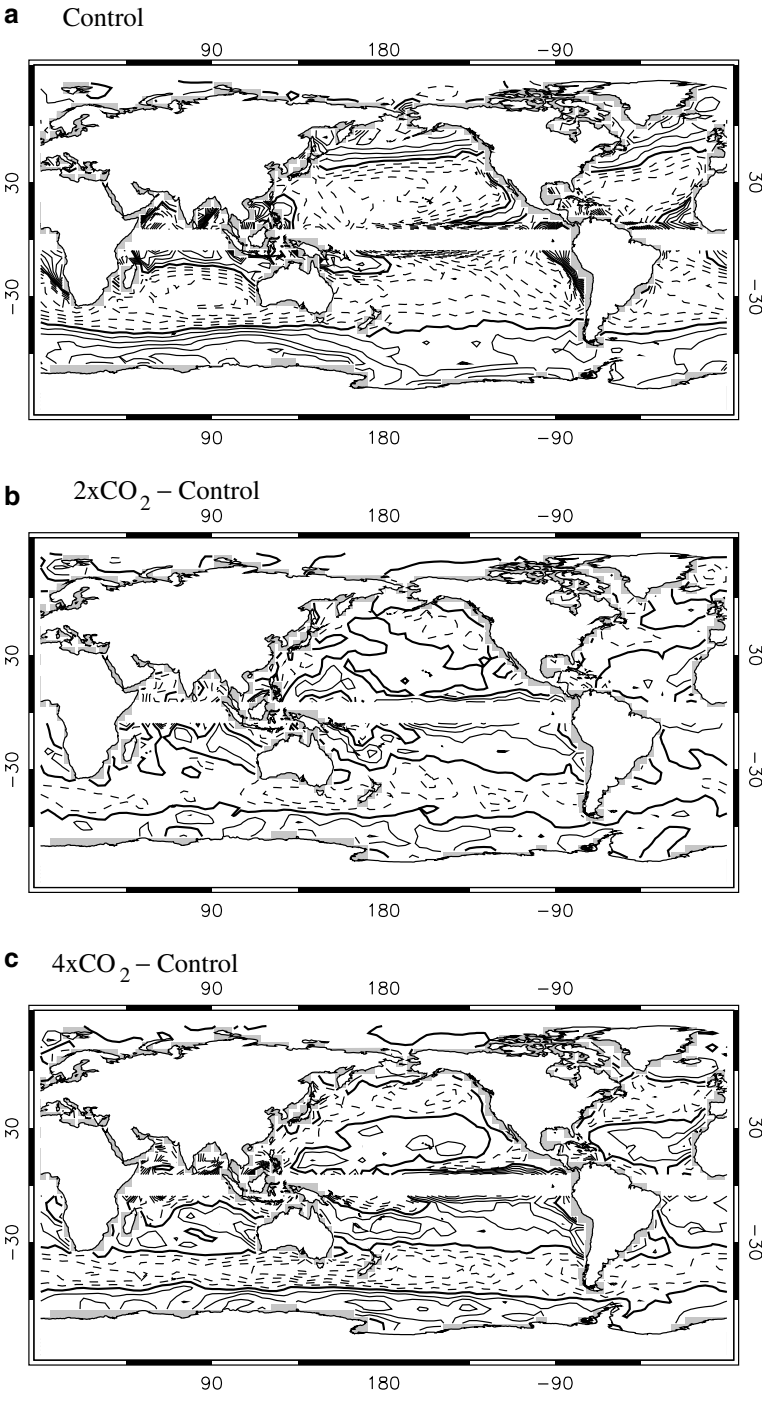

Fig. 5 **a** Ekman pumping in the Control state, **b** Ekman pumping change in the $2\times CO_2$ state ($2\times CO_2$ minus Control) and **c** Ekman pumping change in the $4\times CO_2$ state ($4\times CO_2$ minus Control). Negative values are *dashed*; zero line is *bold*; contour interval is 0.4×10^{-6} m/s in **a** and 0.2×10^{-6} m/s in **b** and **c**

Ekman pumping anomaly becomes positive between roughly 10–30°S and 10–30°N (Fig. 5b, c), indicating a weakening of the subtropical downward pumping. Towards the mid-latitudes, between roughly 30–50°S and 30–50°N, the pumping anomaly becomes negative, as expected from the shift of the wind stress curl profile and the resulting curl anomaly (Fig. 2b). The projected increase in the downward Ekman pumping between about 30–50°S, seen in Fig. 5b, c, deserves special mention. This region north of the ACC accounts for a large fraction of the net uptake of GHGs from the atmosphere in the real ocean, with the Ekman pumping playing an important role in this process. In our experiments, the downward Ekman pumping between 50°S and 30°S (i.e., north of the mean position of zero wind stress curl) increases by 21% at $2\times CO_2$ and by 36% at $4\times CO_2$.

We now consider the horizontal mass transport and its projected changes. To begin with, Fig. 6 compares the total and the Sverdrup mass transport streamfunctions corresponding to the Control state. The former is computed from the full model dynamics, whereas the

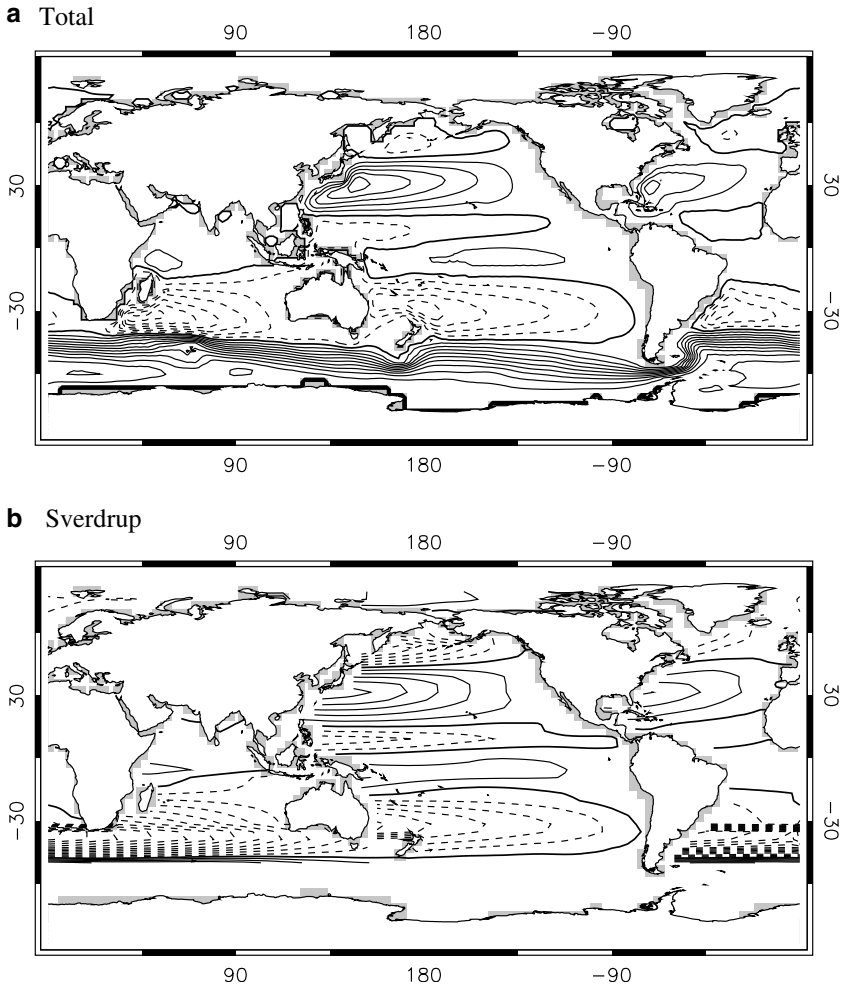

Fig. 6 **a** Total and **b** Sverdrup mass transport streamfunctions corresponding to the Control state. Negative values are *dashed*; zero line is *bold*; contour interval is 10 Sv

Sverdrup transport is computed from Eq. 3 using only the wind stress curl and the values of streamfunction along the eastern boundaries of the oceans. The comparison indicates that the major subtropical gyre systems in the model are essentially in Sverdrup balance. We exploit this fact to interpret the projected changes in the horizontal mass transport in our climate change experiments.

Figure 7 illustrates that the changes in the total horizontal mass transport are in good agreement with the changes implied by the Sverdup balance in most subtropical regions. In particular, the structure and the magnitude of the mass transport anomaly field (Fig. 7a) closely resembles the corresponding changes in the Sverdrup transport (Fig. 7b). This suggests that in these regions, the projected changes in the mass transport are dominated by changes in the local basin-scale wind stress curl. The largest changes in both the total transport and the Sverdrup transport are found in the South Pacific. It is also in the South Pacific where the poleward shift of the position of zero wind stress curl in the mid-latitudes is largest (Fig. 8). We note that the coherent circumpolar shift to the south of zero wind stress curl around Antarctica shown in Fig. 8 is consistent with the poleward shift of the ACC, as seen in the horizontal mass transport anomaly in Fig. 7a. Oke and England (2004) obtain a similar structure of the horizontal mass transport anomaly in the Southern Ocean by imposing an idealized poleward shift of wind stress in an ocean-only general circulation model.

As pointed out in the previous subsection, the changes in the wind stress over the Southern Ocean result in the changes in the oceanic density structure. The changes are not dramatic, but are sufficient to modify the so-called baroclinic potential energy, $\chi(=(g/\rho_o)\int z\tilde{\rho}\mathrm{d}z$, where $\tilde{\rho}$ is the density minus a horizontal mean density profile—e.g. see Borowski et al. 2002), and hence the ACC mass transport. As shown in Borowski et al. (2002), given relatively small near-bottom velocities and near steady state, one should expect the following relation between a change in the ACC transport, $\Delta\varphi$, and a change in the baroclinic potential energy, $\Delta\chi$: $\Delta\varphi = \Delta\chi/f_o$,where f_o is the Coriolis parameter taken at the mean latitude of the ACC. Figure 9 illustrates this connection. By the time the atmospheric CO_2 concentration reaches four times of its initial value, mass transport between 47°S and 62°S at 130°E (between Australia and Antarctica) increases by about 27 Sv, out of which about 20 Sv is due to the changes in the baroclinic potential energy.

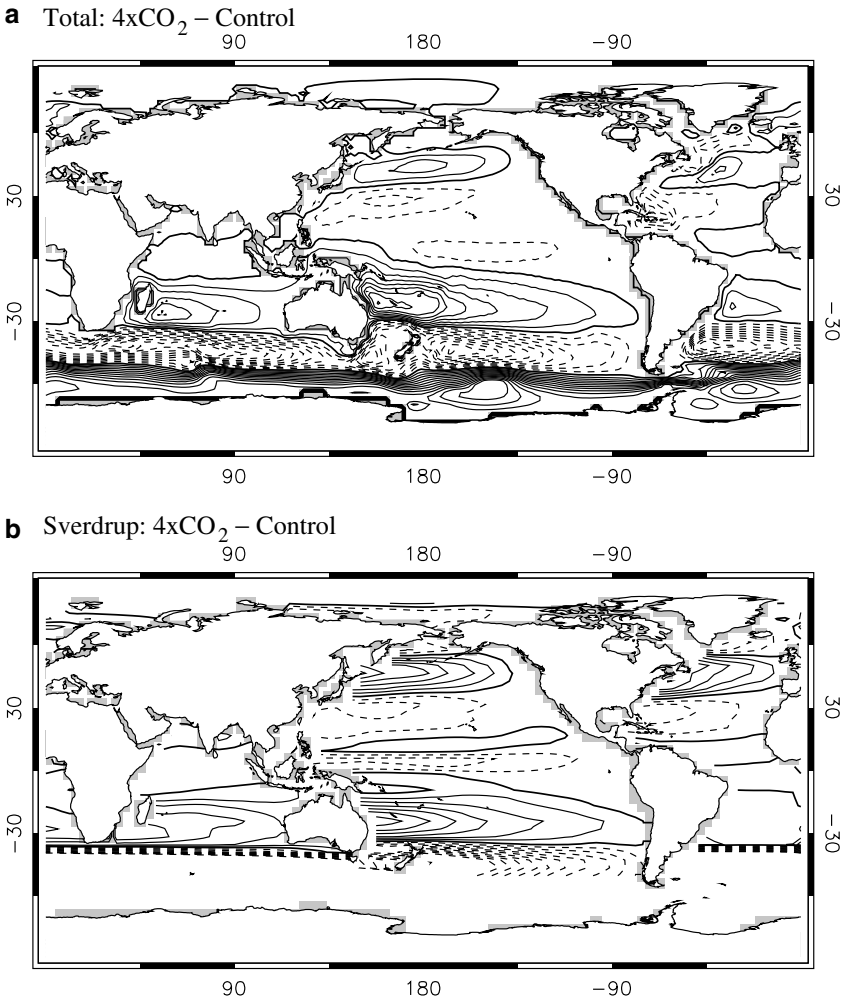

Fig. 7 Changes in **a** total and **b** Sverdrup mass transport streamfunction in the $4\times CO_2$ climate ($4\times CO_2$ minus Control). Negative values are *dashed*; zero line is *bold*; contour interval is 2 Sv. The corresponding transport changes in the $2\times CO_2$ state have a similar spatial structure but weaker magnitude compared to $4\times CO_2$ minus Control

The changes in the ACC in response to the changes in the wind stress, as well as the connection between the meridional and zonal circulation in the Southern Ocean, can be understood by applying the so-called residual-mean theory within the zonally unblocked region of the Southern Ocean (e.g., Karsten et al. 2002;

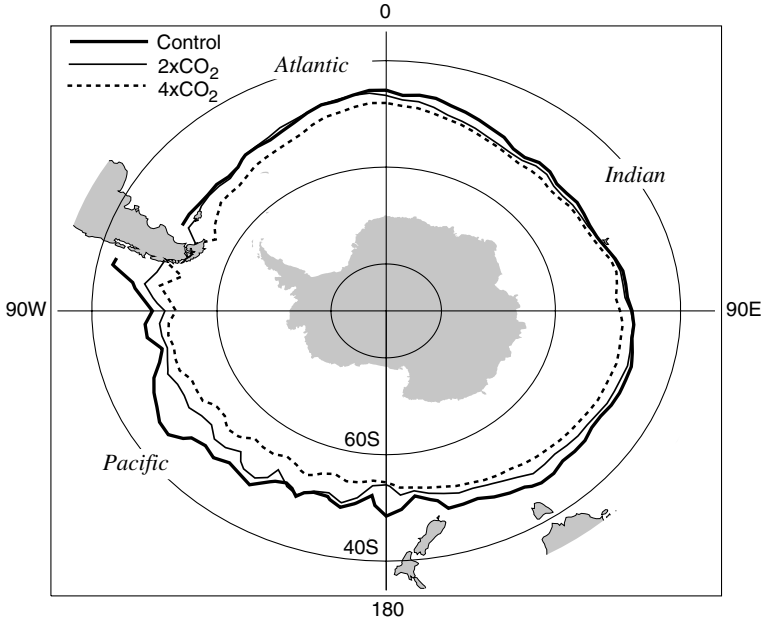

Fig. 8 Position of zero wind stress curl in the mid-latitudes around Antarctica in the model experiments

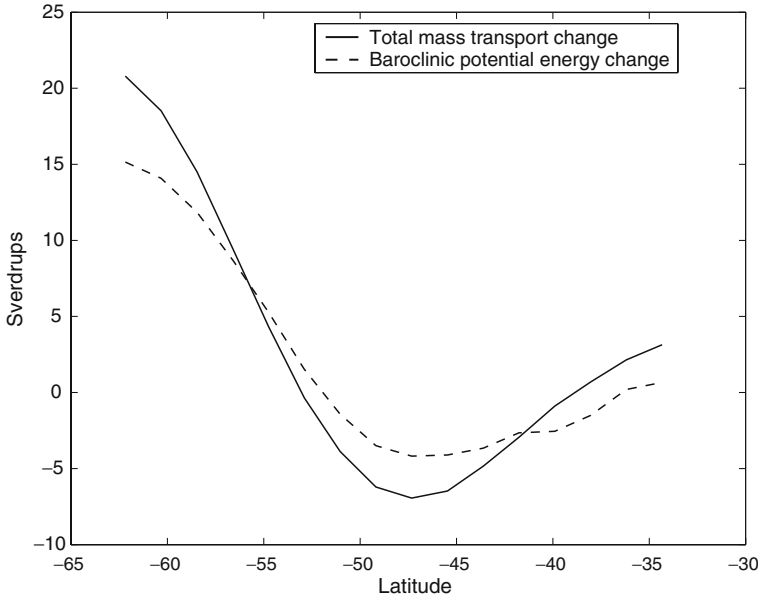

Fig. 9 Changes in the mass transport between Australia and Antarctica (at 130°E) in the $4\times CO_2$ state: total (*solid*) and due to the changes in the baroclinic potential energy (*dashed*)

Marshall and Radko 2003; Rintoul et al. 2001). The theory assumes that the net zonal-mean meridional circulation, or the residual circulation Ψ^r, is given by a difference between the Eulerian meridional circulation, $\overline{\Psi}$, and the eddy-induced circulation Ψ^*, i.e. $\Psi^r = \overline{\Psi} - \Psi^*$. The Eulerian circulation is associated with the northward wind-driven Ekman transport ($\overline{\Psi} = -\bar{\tau}_{\text{zonal}}/f\rho_o$), tending to overturn the isopycnals and increase the potential energy stored in the ACC density front. The eddy-induced circulation, in turn, is generated by a transfer of momentum through the water column by interfacial form stress ($\Psi^* = \overline{\rho' v'}/\bar{\rho}_z$, with the overbar and superscript denoting a zonal mean and its deviation respectively; ρ is the density). In contrast to the Eulerian circulation, the eddy-induced circulation tends to flatten the isopycnals and reduce the potential energy of the ACC density front. These two competing processes set the slope of isopycnals across the ACC and hence its baroclinic transport. Parameterizing the lateral buoyancy transfer by the ACC eddies, $\overline{\rho' v'}$, one can obtain a relation connecting the zonal shear of the ACC, $\bar{u}_z$, to the zonal wind stress such as $\bar{u}_z \sim \bar{\tau}^{\alpha}_{\text{zonal}}$, where α is a positive constant. Although different parameterizations may lead to different values for the α exponent (e.g., Rintoul et al. 2001), all such scaling relations suggest that a meridional shift of zonal winds in the Southern Ocean leads to a similar shift of ACC. In reality, bottom topography exerts a strong constraint on the mean pathway of the ACC flow, so that the actual shift of ACC may be smaller compared to the shift implied by this theoretical argument. Moreover, the residual-mean theory assumes a steady-state balance which may introduce an additional disagreement between the theoretical and the model predictions. However, as shown in FS05, despite these limitations, the agreement between the theoretical and the model predictions of the shift of ACC in response to the shift of winds is remarkably good, holding also for other global coupled climate models.

Many previous studies (e.g., Gent et al. 2001; Bi et al. 2002) found that the changes in the thermohaline circulation off the Antarctic shelf, associated with the formation of bottom water (likely, due to offshore sea-ice motion—see, for example, Saenko et al. 2002), also contribute to the strength of the mean transport of the ACC. In particular, results of Gent et al. (2001) indicate that there is a strong correlation between the transport of the ACC and both the strength of the meridional Ekman transport at the latitude of Drake Passage and the thermohaline circulation off the Antarctic shelf. In our global warming experiments, however, the strength of the thermohaline circulation off the Antarctic shelf decreases, in general agreement with other studies (e.g., Gregory 2000). This rules out the possibility that the strengthening of the ACC transport in our experiments can be explained by the changes in the thermohaline circulation off the Antarctic shelf.

In the subpolar regions of the Northern Hemisphere, the agreement between the changes in the total horizontal mass transport and the changes in the Sverdrup mass transport is poor. There, the assumptions made in the derivation of the Sverdrup balance (e.g., zero bottom velocity), are invalid so that the effects of bottom topography in the vorticity balance become important. This follows since the vertical scale of the flow is $h = Lf/N$, where L is the horizontal scale of the topography and N is the buoyancy frequency. The vertical scale increases with a decrease of stratification implying a deeper penetration of the flow. In the subpolar North Atlantic, where the circulation is known to be sensitive to changes in surface buoyancy flux, the weakening of the deep thermohaline flow in response to the increasing CO_2 level in the atmosphere appears to play the key role in the response of horizontal mass transport there.

4.3 Wind work on the ocean geostrophic currents

Observational estimates indicate that the wind energy input to the surface geostrophic currents is dominated by the product of the time-mean wind stress and the time-mean geostrophic currents (e.g., Wunsch 1998). In agreement with observational estimates, the Southern Ocean is the dominant region of wind energy input in our model (Fig. 10). The model predicts an increase of the work done by the wind stress on the mean geostrophic currents with the increase of CO_2 concentration in the atmosphere. Globally, the increase amounts to 17% at doubled CO_2 and by 32% at quadrupled CO_2. South of 30°S, the wind energy supply is predicted to increase by 22% at $2\times CO_2$ and by as much as 48% at $4\times CO_2$. The latter comes about due to the product of a stronger zonal wind stress and stronger zonal surface geostrophic currents in the Southern Ocean which is equivalent to an increase in the product of northward Ekman transport and the meridional pressure gradient across the ACC. The stronger overall meridional pressure gradient in the Southern Ocean leads to an increase of mass transport through Drake Passage form 95 Sv in the Control climate to 101 Sv at $2\times CO_2$ and to 116 Sv at $4\times CO_2$. An implication of this result is that our model predicts that increasing concentrations of GHGs in the atmosphere will result in more mechanical energy available to drive the ocean circulation.

5 Summary and conclusions

The results of our global warming simulation, following a simple 1% per year CO_2 increase scenario suggest that the surface wind stress and the wind-driven ocean circulation change significantly, particularly by the time the atmospheric CO_2 level reaches four times its present day level. In particular, the mean zonal wind stress at mid-latitudes shifts poleward by a few degrees in both hemispheres. In addition to the poleward shift, the mid-latitude wind stress increases, particularly strongly in the Southern Hemisphere (from 0.17 Pa to 0.21 Pa in the zonal mean at $4\times CO_2$). This results in more intense vertical and horizontal circulations in the Southern Ocean. In this region, the stronger northward transport of relatively light water in the Ekman layer is compensated by stronger southward flow and upwelling of denser deep water around Antarctica. This results in an intensification of the circulation associated with the subpolar overturning cell, between about 60–40°S (by as much as 12 Sv at $4\times CO_2$). Such an intensification of meridional overturning in the Southern Ocean may have a number of physical and biological implications, including an enhanced supply of nutrients to the surface south of ACC due to the intensified upwelling of deep water.

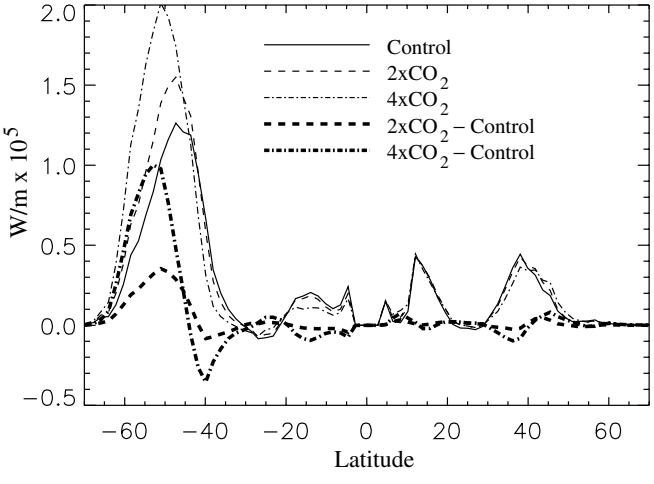

Fig. 10 Zonally-integrated work done by the time-mean winds on the time-mean surface geostrophic currents in the Control climate, the $2\times CO_2$ climate and the $4\times CO_2$ climate. *Heavy lines* show the difference between the climate states experiments and the Control state

These wind stress changes translate into important wind stress curl changes, favoring a poleward expansion of the subtropical gyres. The largest associated changes in the horizontal mass transport are found in the Southern Hemisphere, particularly in the South Pacific. We showed that the simulated changes in the total mass transport in the subtropical regions are dominated by changes in the local basin-scale wind stress curl. In the subpolar regions, however, particularly in the North Atlantic, other physical processes are at play such as, for example, those associated with the deep thermohaline flow.

The simulated changes in wind stress curl force an increase of downward Ekman pumping on the poleward edges of the subtropical gyres. In particular, in the region of intense vertical wind-driven heat transfer at about 50–30°S, the downward Ekman pumping increases by 21% in the state for a doubled CO_2 and by 36% in the state for a quadrupled CO_2. Such an increase may tend to retard the surface warming by removing more heat and GHGs from the surface to the deeper ocean.

Finally, we showed that the increased wind stress, particularly over the region of relatively strong surface currents in the Southern Ocean, results in more work being done by the wind on geostrophic ocean currents. In our experiments, the simulated increase of wind energy input to the large-scale ocean circulation reaches 32% globally and 48% south of 40°S by the time the atmospheric CO_2 level reaches four times its initial level. This suggests a significant re-organization of ocean dynamics in response to GHGs, particularly in the Southern Hemisphere. More global implications of the increase of mechanical energy supply to the ocean (e.g., Huang 2004) might also be possible due to the processes not parameterized in this model version, such as, for example, a dependence of oceanic diapycnal mixing on winds and stratification.

Acknowledgements The authors are indebted to the CCCma coupled modelling group for performing the model simulations. We would like to thank Bill Merryfield, Greg Flato and Jim Christian for useful comments. MHE acknowledges support from the Australian Research Council. Comments from two reviewers helped to improve the paper.

References

Abdella K, McFarlane NA (1997) A new second-order turbulence closure scheme for the planetary boundary layer. J Atmos Sci 54:1850–1867

Bi D, Budd WF, Hirst AC, Wu X (2002) Response of the antarctic circumpolar current transport to global warming in a coupled model. Geophys Res Lett 29. DOI 10.1029/2002GL015919

Boer GJ, Flato G, Ramsden D (2000) A transient climate change simulation with greenhouse gas and aerosol forcing: projected climate for the twenty-first century. Clim Dyn 16:427–450

Borowski D, Gerdes R, Olbers D (2002) Thermohaline and wind forcing of a circumpolar channel with blocked geostrophic contours. J Phys Oceanogr 32:2520–2540

Cubasch U, Meehl GA, Boer GJ, Stouffer RJ, Dix M, Noda A, Senior CA, Raper S, Yap KS et al (2001) Projections of future climate change. In: Climate change 2001. The Scientific Basis Contribution of Working Group I to the Third Assessment Report of the Intergovernmental Panel on Climate Change. Cambridge University Press, Cambridge, pp 525–582

Danabasoglu G (1998) On the wind-driven circulation of the uncoupled and coupled NCAR climate system ocean model. J Clim 11:1442–1454

Döös K, Webb DJ (1994) The Deacon Cell and the other meridional cells in the Southern Ocean. J Phys Oceanogr 24:429–442

Flato GM, Hibler WD III (1992) Modeling pack ice as a cavitating fluid. J Phys Oceanogr 22:626–651

Flato GM, Boer GJ, Lee WG, McFarlane NA, Ramsden D, Reader MC, Weaver AJ (2000) The Canadian Centre for climate modeling and analysis global coupled model and its climate. Clim Dyn 16:451–467

Fofonoff NP (1981) The Gulf Stream system. In: Honor of Henry Stommel, Warren BA, Wunsch C (eds) Evolution of physical oceanography scientific surveys. The MIT Press, Cambridge, pp 112–139

Fyfe JC (2003) Extratropical Southern Hemisphere cyclones: harbingers of climate change? J Clim 16:2802–2805

Fyfe JC, Saenko OA (2005) Human-induced change in the Antarctic circumpolar current. J Clim (in press)

Gent PR, McWilliams JC (1990) Isopycnal mixing in ocean general circulation models. J Phys Oceanogr 20:150–155

Gent PR, Large WG, Bryan FO (2001) What sets the mean transport through Drake passage? J Geophys Res 106:2693–2712

Gillett NP, Zwiers FW, Weaver AJ, Stott PA (2003) Detection of human influence on sea level pressure. Nature 422:292–294

Gregory JM (2000) Vertical heat transports in the ocean and their effect on time-dependent climate change. Clim Dyn 15:501–515

Hellerman S, Rosenstein M (1983) Normal monthly wind stress over the world ocean with error estimates. J Phys Oceanogr 13:1093–1104

Huang RX (2004) Ocean, energy flow. In: Cleveland CJ (ed) Encyclopedia of energy. Elsevier, Amsterdam 4:497–509

IPCC (2001) Climate change 2001. The scientific basis: summary for policymakers, Part of the Working Group I contribution to the 3rd Assessment Report of the Intergovernmental Panel on Climate Change, Cambridge University Press, Cambridge

Karsten R, Jones H, Marshall J (2002) The role of eddy transfer in setting the stratification and transport of a circumpolar current. J Phys Oceanogr 32:39–54

Marshall GJ (2003) Trends in the southern annular mode from observations and reanalyses. J Clim 16:4134–4143

Marshall J, Radko T (2003) Residual-mean solutions for the Antarctic Circumpolar Current and its associated overturning circulation. J Phys Oceanogr 33:2341–2354

McFarlane NA, Boer GJ, Blanchet J-P, Lazare M (1992) The Canadian climate centre second-generation general circulation model and its equilibrium climate. J Clim 5(10):1013–1044

McFarlane NA, Scinocca JF, Lazare M, Verseghy D, Li J, Harvey R (2004) The Canadian climate centre third-generation atmospheric general circulation model. (in preparation)

Oke PR, England MH (2004) On the oceanic response to changes in the latitude of the Southern Hemisphere subpolar westerly winds. J Clim 17:1040–1054

Pacanowski RC, Dixon K, Rosati A (1993) The GFDL modular ocean model users guide. In: GFDL Ocean Group Technical Report 2. Geophysical Fluid Dynamics Laboratory, Princeton, 46 pp

Rintoul SR, Hughes CW, Olbers D (2001) The Antarctic Circumpolar Current system. In: Siedler G, Church J, Gould J (eds) Ocean circulation and climate, Academic, London, chap 4.6, 715 pp

Saenko OA, Schmittner A, Weaver AJ (2002) On the role of wind-driven sea ice motion on ocean ventilation. J Phys Oceanogr 32:3376–3395

Speer K, Guilyardi E, Madec G (2000a) Southern Ocean transformation in a coupled model with and without eddy mass fluxes. Tellus 52A:554–565

Speer K, Rintoul SR, Sloyan B (2000b) The diabatic Deacon Cell. J Phys Oceanogr 30:3212–3222

Trenberth KE, Olson JG, Large WG (1989) A global ocean wind stress climatology based on ECMWF analysis, NCAR Technical Note, NCAR/TN-338 + STR, 93 pp

Wunsch C (1998) The work done by the wind on the oceanic general circulation. J Phys Oceanogr 28:2332–2340